Journal of Power Sources 266 (2014) 179–185

Contents lists available at ScienceDirect

Journal of Power Sources

journal homepage: www.elsevier.com/locate/jpowsour

Fabrication and electrochemical characterization of amorphous lithium iron silicate thin films as positive electrodes for lithium batteries

I. Quinzeni [a], S. Ferrari [a,*], E. Quartarone [a], D. Capsoni [a], M. Caputo [b], A. Goldoni [b], P. Mustarelli [a], M. Bini [a]

[a] Dept. of Chemistry, University of Pavia, Viale Taramelli 16, 27100 Pavia, Italy
[b] Elettra Sincrotrone Trieste, Strada Statale 14, Km 163.5, I-34149 Trieste, Italy

HIGHLIGHTS

- Thin film deposition of amorphous Li/M(Fe,Mn)/Si/O by r.f. sputtering.
- Good electrochemical performances: 50 mAh g^{-1} at 2.5 C.
- The films were able to sustain about 300 cycles of charge–discharge.

GRAPHICAL ABSTRACT

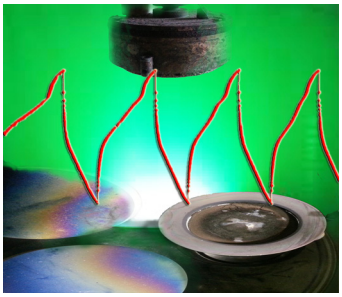

ARTICLE INFO

Article history:
Received 22 January 2014
Received in revised form
25 April 2014
Accepted 3 May 2014
Available online 13 May 2014

Keywords:
Lithium microbattery
Thin film
r.f. sputtering
Li_2FeSiO_4
XPS
Cyclic voltammetry

ABSTRACT

In this work we reported, for the first time, the preparation by radio frequency sputtering and the electrochemical characterization of Li/M/Si/O thin films (M = Fe, Mn), as positive electrodes for lithium microbatteries. The deposited films were amorphous both in case of pure iron and mixed iron/manganese compositions. The electrochemical performances, in terms of capacity values and coulombic efficiency, were comparable to those currently reported for the corresponding crystalline bulk materials. In particular, capacities of the order of 50 mAh g^{-1} were obtained at 2.5 C with coulombic efficiency near 90% by using a standard liquid electrolyte. Our preliminary electrochemical results, together with the easiness of preparation, suggested that Li/M/Si/O thin films could be interesting candidates as cathodes in lithium microbatteries.

1. Introduction

The development of thin-film lithium batteries as power sources for new generation micro-devices was rapidly growing over these last years. Such microsystems show several advantages, e.g. lightness, low cost and easy integration in micro-devices owing to their miniaturization [1,2]. A wide area of applications may be foreseen, ranging from microelectronics to sensors in medical and

* Corresponding author. Dipartimento di Chimica, Sezione di Chimica Fisica, Università di Pavia, Viale Taramelli 16, 27100 Pavia, Italy. Tel.: +39 382 987213; fax: +39 382 987575.
E-mail addresses: stefania.ferrari@unipv.it, S.Ferrari@warwick.ac.uk (S. Ferrari).

http://dx.doi.org/10.1016/j.jpowsour.2014.05.012
0378-7753/

military fields, smart cards and other micro-devices (MEMS, NEMS), and also Radio Frequency Identification (RFID) tags, and this represents a very topical target. Large-scale applications in the next future are chiefly expected for food and drug control. During the last years, many efforts on the optimization of lithium microbatteries were discussed in the literature, regarding both flat [Ref. [3] and references therein] and 3D configurations [4].

Many materials were suggested in the past as microbattery components, such as V_2O_5 [5], $LiCoO_2$ [6,7] or $LiMn_2O_4$ [8,9] as high voltage cathodes, lithium oxide or sulphide compounds (crystals and glasses) as solid electrolytes [10], and Li metal or vanadates [11] as the anodes. The use of thin film electrodes to shorten diffusion paths of Li ions seems to be an effective solution to enhance the rate capability of a battery, but the energy density still remains a challenge. A recently proposed solution encompassing both high energy and high power densities is the development of three-dimensional (3D) nanostructured architectures and design with large surface area [12–14]. However, there are still two major obstacles for wider applications of the 3D electrodes. The first one is the complex and high-cost fabrication process, that limits the large-scale production. The other is that the energy density of the whole device is still low, due to the extremely thin active material layer as compared with the much thicker substrate.

Moreover, increasingly important safety and toxicity issues should be considered, which are chiefly relevant in case of $LiCoO_2$ and $LiMn_2O_4$, the most used compounds for thin film cathode preparation. Therefore, more environmentally friendly compounds are required for these applications. In this frame, $LiFePO_4$ belonging to the family of polyanion compounds is important because, among other fundamental properties such as the good cycling stability, it is highly safe and non-toxic. Thin films of $LiFePO_4$ have been prepared by different deposition techniques such as r.f. sputtering [15], electrophoretic deposition [16] and pulsed laser deposition [17], and the effects of deposition temperature and kind of substrate on the crystal structure and morphology of the resulting thin films have been already addressed.

Recently, low toxic, low cost and highly available cathode materials belonging to the orthosilicate family with formula Li_2MSiO_4 (M = Fe, Mn) were proposed as bulk materials [18–20]. Several works were devoted to their structural and computational characterization [21–24], as well as to the optimization of their electrochemical performances [25]. The importance of these compounds chiefly resides in their high theoretical capacity (up to 330 mAh g^{-1} for two lithium ions insertion/extraction) that justifies the efforts devoted to the preparation of new architectures such as nano- and mesoporous forms [26–28]. In case of standard Li-ion cells, orthosilicates (e.g. Li_2MnSiO_4) are generally prepared and used in crystalline form, but they can undergo amorphization on repeated cycling [29]. This crystalline-to-amorphous transition, in turn, leads to a progressive worsening of the electrochemical performances. So far, the preparation of orthosilicate thin films was never reported, likely due to the difficulty to deposit with the right stoichiometry a ternary oxide, differently from binary compounds such as vanadium [30], titanium [31] and iron oxides [32].

In this work, for the first time to our knowledge, we reported the radiofrequency (r.f.) magnetron sputtering preparation and the physico-chemical characterization of Li/M/Si/O (M = Fe, Mn) amorphous films with nominal composition $Li_2Fe_{1-x}Mn_xSiO_4$ (x = 0, 0.5). The structural and microstructural properties of the thin films were investigated by means of XRD, SEM and XPS techniques. The electrochemical properties were addressed by performing cyclic voltammetry and preliminary battery tests on a lithium cell with a standard liquid electrolyte.

2. Experimental

2.1. Synthesis

Thin films with nominal composition $Li_2Fe_{1-x}Mn_xSiO_4$ ($x = 0, 0.5$) were deposited in a high vacuum (10^{-3} Pa) r.f. magnetron sputtering system, which consists of three confocal cathodes at 40–50 mm from the substrate center. As the deposition substrates, we used stainless steel (s.s.) disks with a diameter of 10 mm (Good Fellow, SS-AISI304 Fe/Cr18/Ni10 annealed), previously coated by a 150 nm-thick layer of gold as current collector. $Li_2Mn_{0.5}Fe_{0.5}SiO_4$ and Li_2FeSiO_4 powders, prepared by sol–gel synthesis [20,21], were used as the target. The depositions were performed by a procedure made of two consecutive steps without sample extraction: 1) at 60 W for 1 h; 2) at 100 W for 2 h. The pressure was kept at $3 \cdot 10^{-2}$ mbar, with a substrate temperature of 700 °C and 20 sccm of Ar flow. At the end of the deposition, the samples were kept at the same temperature (700 °C) for additional 1 h inside the r.f. sputtering chamber, and then cooled down to ambient temperature under vacuum. The thickness of both the films was about 390 nm, as determined by profilometry. The samples were named FeMn or Fe for the mixed or iron silicate, respectively.

2.2. Characterization techniques

X-ray diffraction (XRD) measurements were performed using a Bruker D5005 diffractometer with the CuKα radiation, a graphite monochromator and a scintillation detector. The patterns were collected with a step size of 0.02° and counting time of 6 s per step in the angular range 15–65°/2θ.

Scanning Electron Microscopy (SEM) measurements were performed with a Zeiss EVO®-MA10-HR microscope.

The film thickness was measured by means of a stylus profilometer (KLA Tencor P6 Profiler), by applying a force of 20 μN. The active mass of the silicate thin films (about 30 μg i.e. 60 μg/cm^2) was measured by using an ultra sensitive microbalance (HIDEN ISOCHEMA IGA-001).

X-ray Photoelectron Spectroscopy (XPS) spectra were acquired on a sample deposited in the same way as FeMn on Ni substrate, in order to avoid the signal of Fe coming from stainless steel. XPS spectra were acquired *ex situ* by inserting the sample in a modified VG ESCALAB MkII system, with a base pressure of 10^{-10} mbar, equipped with a non-monochromatic Al Kα X-ray source. The photoelectrons were collected with an hemispherical energy analyzer working at pass energy 10 eV with an energy resolution of 0.9 eV. Sample surface was not treated in any way before the measurements. Si2p has been taken as energy reference in its silicate form (102 eV) [33], after this the binding energy of all the other peaks has been checked and was considered consistent.

The electrochemical tests were performed using a three-electrodes T-cell with lithium metal as the negative and the counter electrodes and a glass-wool (Whatman GF/A) disc as the separator. The electrolyte was 1 M $LiPF_6$ in ethylene carbonate/diethyl carbonate (EC/DEC) 1:1 (Merck). All the cells were assembled in a dry-box under Argon atmosphere. Cyclic voltammetry (CV) was performed by using an Autolab PGSTAT30 (Eco Chemie) at a scan rate of 0.2 mV s^{-1} in the potential range 2.5–4.0 V. The galvanostatic cycling tests were carried out at ambient temperature in the range 2.5–4.5 V using an Arbin battery cycler (model BT-2000).

3. Results and discussion

3.1. Film microstructure and composition

The target materials were thoroughly characterized before to proceed to thin films deposition. The crystalline nature of the

starting powders, as well as structural parameters were determined by XRD [20,21]. Fig. 1 shows the diffraction patterns of the Fe and FeMn thin films. For both the as-prepared films no peaks pertinent to the silicate phase were detected, so we can assume that the films are totally amorphous. Only the peaks due to the gold layer and to the stainless steel substrate are clearly visible (see Fig. 1).

Fig. 2 reports the SEM images of the as-deposited films. The FeMn sample (Fig. 2a) is constituted by two types of particles of different shapes: the film surface is composed by worm-like particles, about 1 μm long and 100–200 nm wide, whereas the part in contact with the substrate is constituted by rounded particles. This layered morphology could be due to the deposition procedure, which comprised two successive steps with different power. In the case of Fe sample (Fig. 2b), the morphology is very different from the one of FeMn, but is again constituted by two different layers: the lower formed by a compact aggregate of small rounded particles and the upper one by bigger particles randomly distributed on the underlying layer.

In order to investigate the composition of the film and the oxidation state of the metal cations, XPS analysis was performed on the FeMn sample. The wide range spectrum (see Fig. 3a) showed peaks of the expected ions pertaining to the orthosilicate target, together with the peak of carbon and Ni. The carbon is a common contaminant for sample growth *ex situ*, while the Ni signal comes from the outer circular ring of the substrate, not covered by the thin film, but completely lightened by the X-ray source and seen by the electron analyzer. Anyway, we cannot exclude the occurrence of an intermixing between Ni and the top $LiMSiO_4$ layer after diffusion of Ni through the Au layer, that could also explain the presence of Ni^{2+} on the cathode surface. For a more detailed analysis, we performed acquisitions of small spectral regions, in the range of the binding energy of the Fe2p (Fig. 3b) and of Li1s, Fe3p and Mn3p one (Fig. 3c). A Shirley-type background was subtracted from each peak and the area subtended by the peak was calculated. Finally, each area was normalized and the intensity of each peak was compared, obtaining the Fe:Mn 2:1 ratio among the elements. Analyzing the Fe2p peaks with their fine structure, that is the fingerprint of the oxidation state of the species, we determined the Fe oxidation state. $Fe2p_{3/2}$ peak has a binding energy of 711.8 eV with a satellite at 718.6 eV, in good accordance with the Fe^{3+} state. For Mn we can base our result just on the binding energy of the $2p_{3/2}$ peak. Its energy is 641.1 eV, in good agreement with Mn^{2+} state. Special care was taken for Li1s peak; in fact, its binding energy is very close to that of the Fe3p one, resulting in just one visible peak. Fig. 3c shows the peak and the fit we performed to separate the two components. This way we were able to evidence the Li presence. Then, we have direct evidence of Fe^{3+} formation, even if only Fe^{2+} should be present for the $Li_2Mn_{0.5}Fe_{0.5}SiO_4$ compound. Anyway, we stress here that XPS probes just the topmost atomic layers (10 nm) so Fe^{3+} is detected on the film surface, and it is likely due to air exposure. In addition, intermixing with elements from the SS substrate, such as Fe and Cr, could have been occurred. This aspect is worth to be investigated in future works.

3.2. Electrochemical properties

The cyclic voltammetry (CV) curves of the Fe and FeMn samples are reported in Fig. 4a and b, respectively. In the case of the Fe film, only one peak is clearly seen during both the anodic and cathodic scans. The oxidation peak at about 3.5 V slightly shifts towards higher voltages by increasing the cycle number. The peak current increases up to the third cycle, then remains stable for the successive cycles. The reduction peak at about 3.2 V seems to shift towards lower values during the 6th cycle.

A similar CV plot was obtained for the FeMn sample (see Fig. 4b) where again a single peak at about 3.4 V was seen at positive currents and at about 3.2 V at negative currents. The reversibility of the intercalation/deintercalation process was so proved for both the thin films. The CV profile of the films is very similar to that found for our target materials, where a peak ascribable to the electron transfer reaction in which Fe^{2+} oxidizes to Fe^{3+} is observed at almost the same potentials (see inset of Fig. 4a and b). Therefore, we can conclude that the films are able to intercalate and deintercalate Li^+ during the electrochemical cycling. These results also give an indirect and circumstantial evidence that the amorphous phase is retaining the lithium orthosilicate composition.

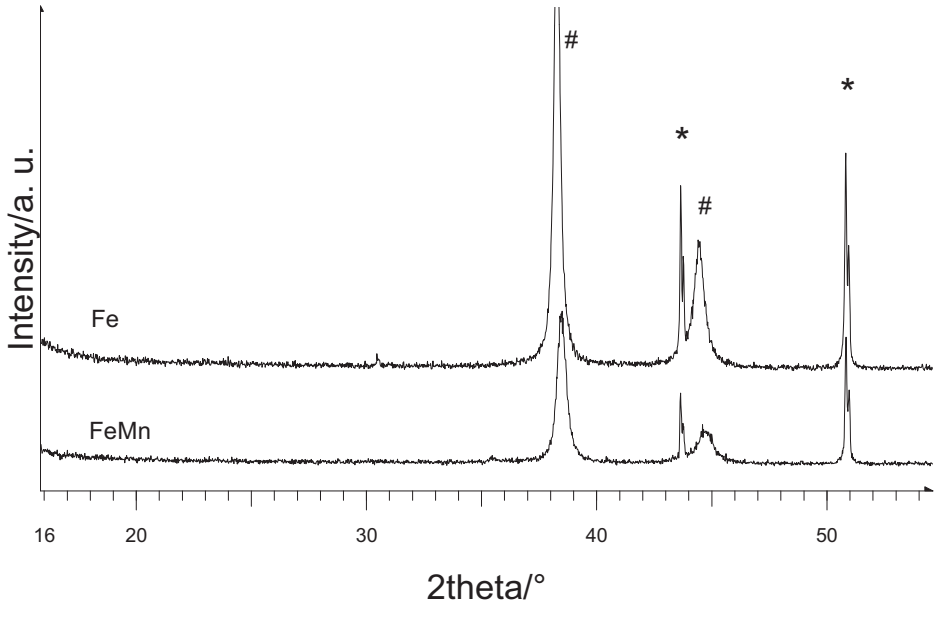

Fig. 1. XRD patterns of the as-deposited Fe and FeMn thin films (* indicate SS substrate reflections and # the gold ones).

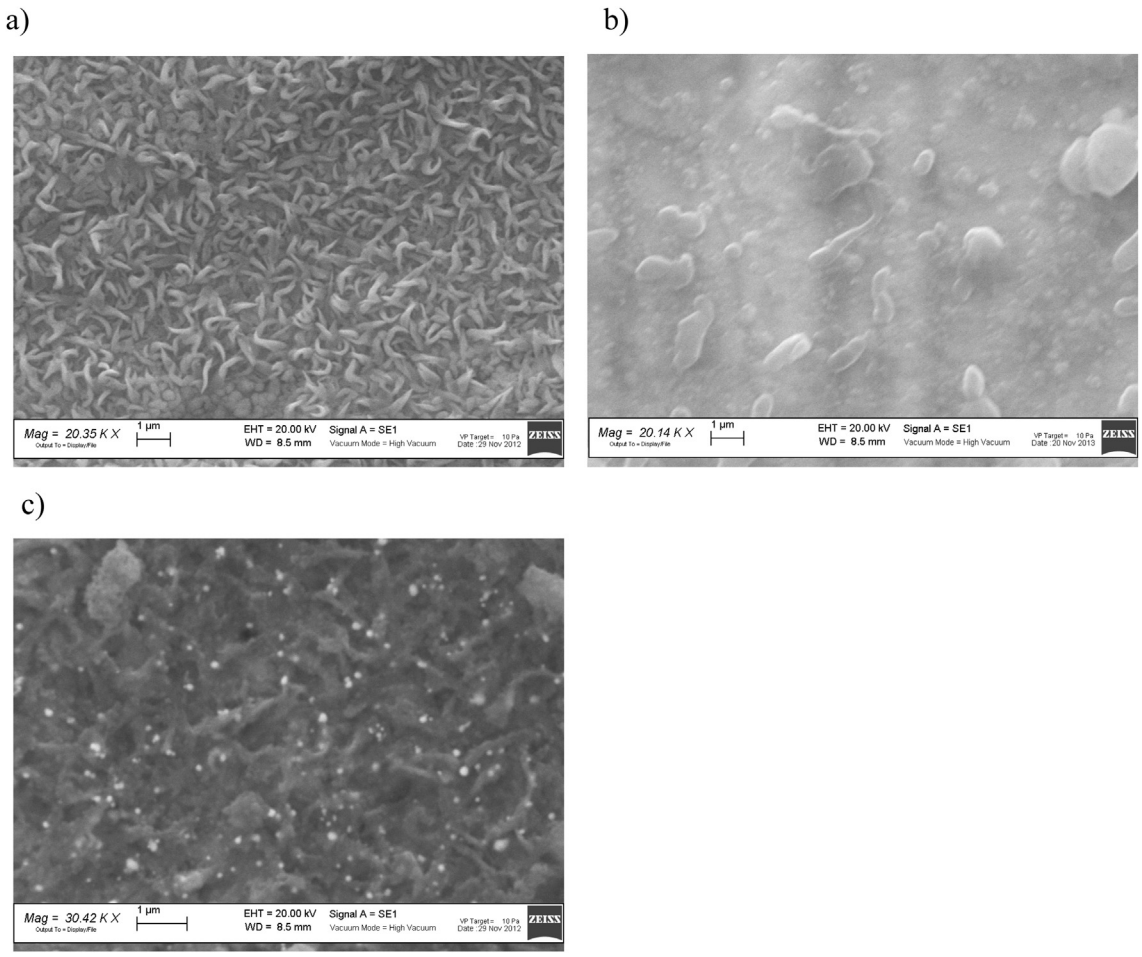

Fig. 2. SEM micrographs of a) as-deposited FeMn, b) as-deposited Fe thin film, c) FeMn thin film after galvanostatic charge–discharge cycling.

The thin films were then tested by galvanostatic charge/discharge measurements, and their performances are reported in Fig. 5a and b. The Fe sample (Fig. 5a) could deliver an initial charge capacity of about 170 mAh g^{-1} for the first cycles at 0.5 C, then the current was raised at 1 C and capacity values around 50 mAh g^{-1} were observed. After 75 cycles, the same galvanostatic test was repeated to check the cell response to repeated cycling, and we obtained a maximum charge capacity of 140 mAh g^{-1} at 0.5 C, which faded immediately in the successive cycles at the same current. However, at current as high as 2.5 C, and after more than 250 cycles, the cell was still able to deliver about 50 mAh g^{-1} with a coulombic efficiency higher than 90% (see Fig. 5a). A very similar behavior was observed for the FeMn sample (Fig. 5b) for which, after an initial very high charge capacity of about 250 mAh g^{-1}, a decrease towards values of about 50 mAh g^{-1} was obtained for 2.5 C current. Noteworthy, at the lower current of 0.5 C, this sample showed a better performance than the Fe one, but with a lower coulombic efficiency (between 70 and 80% at 0.5 C, see Fig. 5b). For microbatteries is also very important to know capacity and current density per surface unit, and the values corresponding to the first cycle at each current density for the last part of the galvanostatic test are reported in Fig. 5c. The calculated values are quite low, but this is not surprising since this is a well known problem of electrodes in form of thin films, for which new 3D architectures has been recently proposed [12–14].

Generally speaking, the observed lower coulombic efficiency with respect to the corresponding target materials may be explained by considering the amorphous nature of the silicate, for which the lacking of a stable crystalline structure can make the Li^+ intercalation/deintercalation process less reversible. After the cycling measurements, the thin film morphology for the FeMn film appears different from the as-prepared sample (Fig. 2c). In particular, the bright, rounded particles could be the lithium salt of the electrolyte, but what is really evident is the formation of a compact layer in which the worm-like particles are not seen anymore. On the other hand, the use of amorphous active materials could help to achieve higher capacity and cyclability, thanks to the presence of additional stable sites for lithium ions, considering the open and random structure typical of amorphous materials. For example, amorphous MoO_2 exhibited better rechargeability than crystalline MoO_2 [34]. Recently, it was also shown that amorphous TiS_3 has better electrochemical properties than its crystalline counterpart, because it retained its structure during the first tests [35]. In this frame, it is helpful to test amorphous thin films as cathode materials. This could also lead to better interfacial properties towards glassy thin film electrolytes such as LIPON. It should be also pointed out that the cycling performances are generally improved when the electrode is covered by a solid-state electrolyte as often reported in the literature [5,36–38]. For our thin films the observed degradation of the capacity retention may partly result from the use of a liquid electrolyte. In addition, the use of EC/DEC up to 4.5 V may contribute to the losses. A liquid electrolyte based on EC/DMC, that can withstand higher voltages up to 4.5–4.6 V, could help in improving the cell performances.

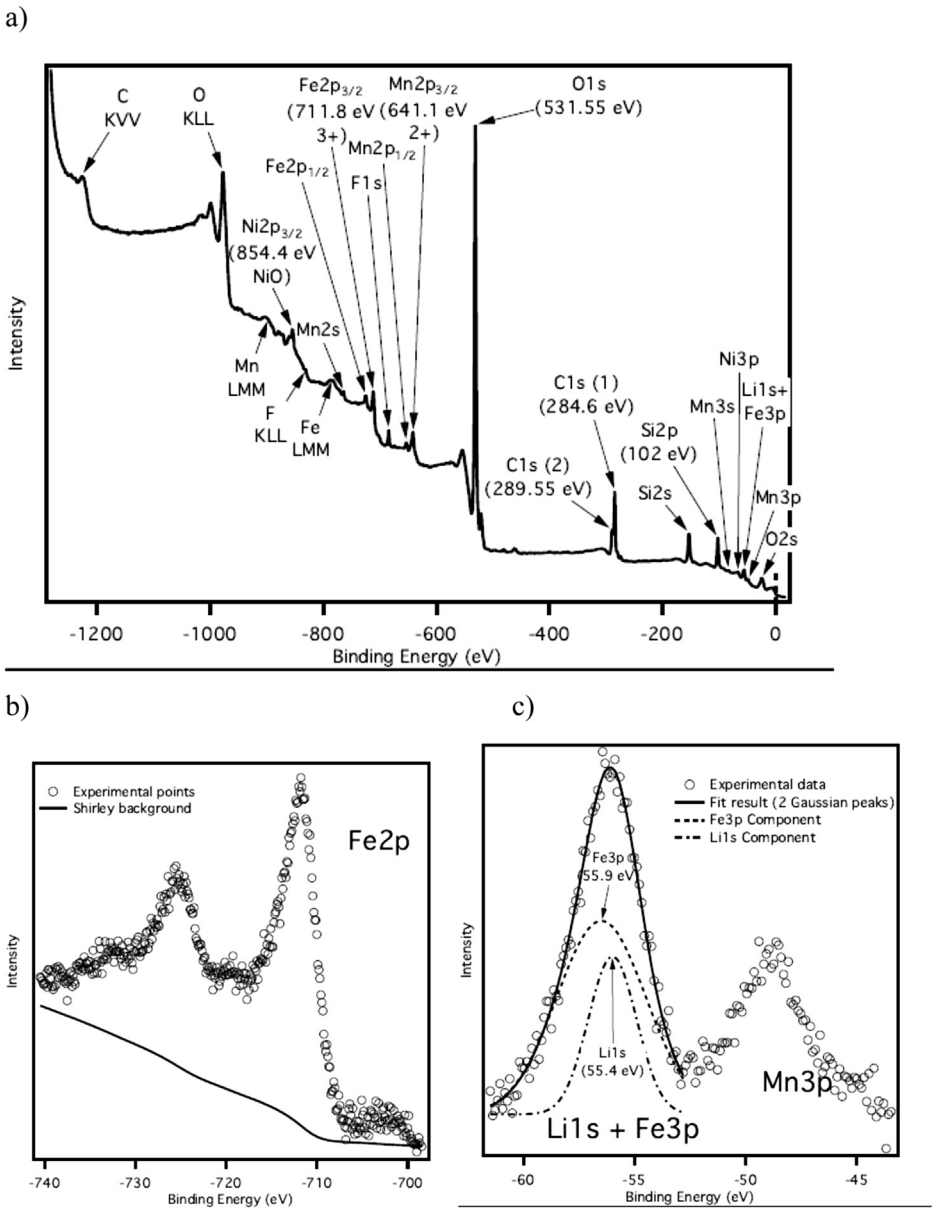

Fig. 3. XPS of FeMn sample: a) wide range spectrum, b) $Fe2p_{3/2}$ photoemission peak, c) Li1s, Mn3p and Fe3p peaks.

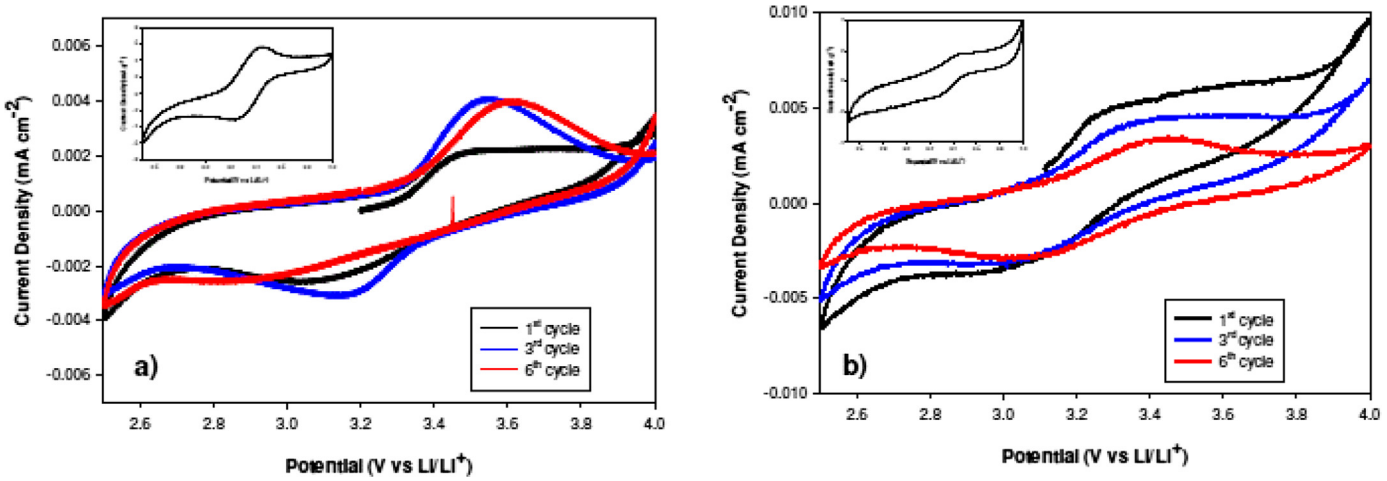

Fig. 4. Cyclic voltammetry plots of a) Fe and b) FeMn samples recorded at 0.2 mV s^{-1} between 2.5 and 4 V. The inset shows CV plots of Fe and FeMn target bulk materials.

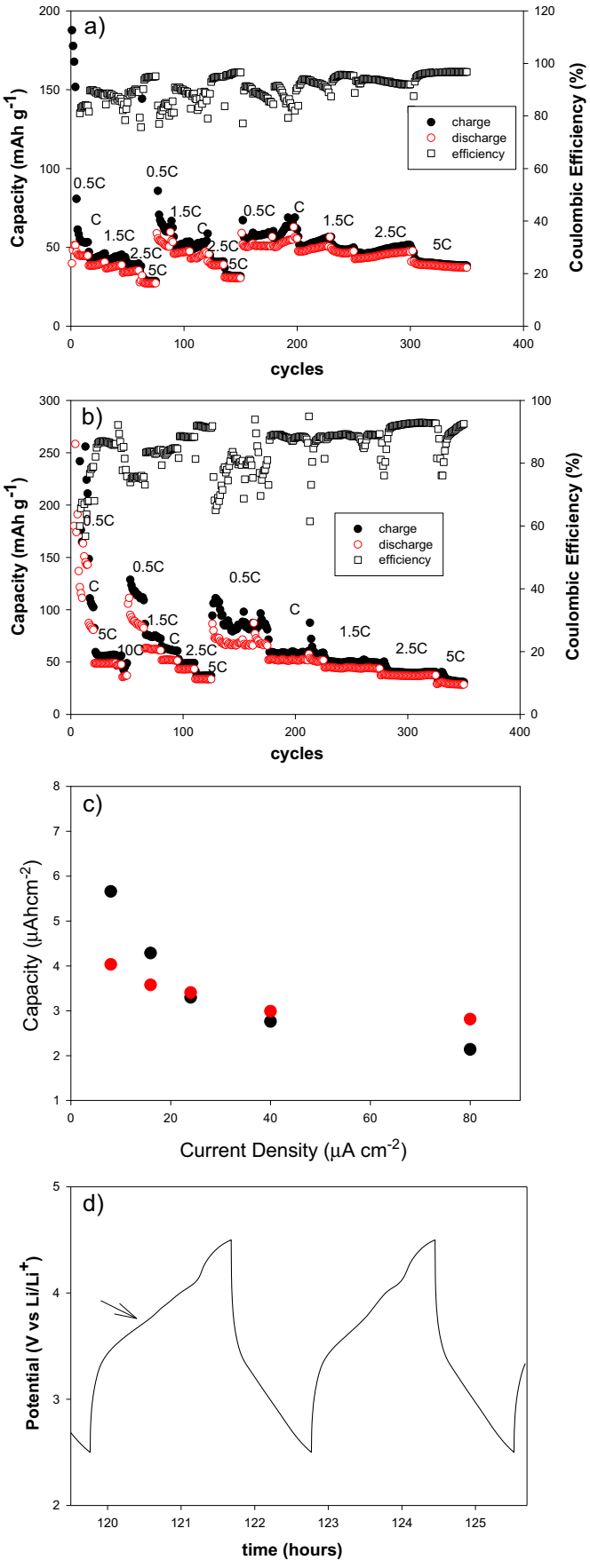

The chronopotentiograms of the FeMn sample are reported in Fig. 5d. In accordance with the CVs, the chronopotentiograms showed a reversible plateau at about 3.5 V, that is clearly visible at least at low current rates, whereas in the charge curve it is less marked. This fact suggests that the Li^+ extraction could proceed in a continuous way, as expected for amorphous materials, rather than with the formation of well-defined phases as expected for crystalline compounds.

4. Conclusions

We successfully deposited lithium iron and iron/manganese orthosilicate amorphous thin films by r.f. sputtering, and preliminary demonstrated their suitability as positive electrodes for lithium batteries. Our films were able to sustain more than 300 galvanostatic cycles with encouraging performances.

Anyway, further improvements can be envisaged by optimizing the deposition parameters such as r.f. power and deposition time, to obtain also crystalline films and to assess their properties with respect to those of the amorphous ones. A future goal is to prepare orthosilicate films with the chance to extract two lithium ions, so obtaining higher capacities and efficiencies.

Acknowledgments

This work was performed in the frame of Cariplo Project 2011-0325 “New electrolyte and electrode materials for thin-film lithium microbatteries”. We kindly thank Mr. Alessandro Girella for the SEM analyses.

References

[1] J.F.M. Oudenhoven, L. Baggetto, P.H.L. Notten, Adv. Energy Mater. 1 (2011) 10–33.
[2] W. Lai, C.K. Erdonmez, T.F. Marinis, C.K. Bjune, N.J. Dudney, F. Xu, R. Wartena, Y.-M. Chiang, Adv. Mater. 22 (2010) E139–E144.
[3] A. Patil, V. Patil, D.W. Shin, Ji-Won Choi, D.-S. Paik, S.-J. Yoon, Mater. Res. Bull. 43 (2007) 1913–1942.
[4] J.W. Long, B. Dunn, D.R. Rolison, H.S. White, Chem. Rev. 104 (2004) 4463–4492.
[5] C. Gerbaldi, M. Destro, Jijeesh R. Nair, S. Ferrari, I. Quinzeni, E. Quartarone, Nano Energy 2 (2013) 1279–1286.
[6] C. Navone, S. Tintignac, J.P. Pereira-Ramos, R. Baddour-Hadjean, R. Salot, Solid State Ionics 192 (2011) 343–346.
[7] E. Ferg, R.J. Gummow, A. de Kock, M.M. Thackeray, J. Electrochem. Soc. 141 (1994) L147–L150.
[8] M. Roberts, P. Johns, J. Owen, D. Brandell, K. Edstrom, G. El Enany, C. Guery, D. Golodnitsky, M. Lacey, C. Lecoeur, H. Mazor, Emanuel Peled, E. Perre, M.M. Shaijumon, P. Simonc, P.-L. Taberna, J. Mater. Chem. 21 (2011) 9876–9890.
[9] P. Birke, W.F. Chu, W. Weppner, Solid State Ionics 93 (1997) 1–15.
[10] S.D. Jones, J.R. Akridge, F.K. Shokooki, Solid State Ionics 69 (1994) 357–368.
[11] M.V. Reddy, B. Pequenard, P. Vinatier, A. Levasseur, J. Phys. Chem. B 110 (2006) 4301–4306.
[12] K. Xie, Z. Lu, H. Huang, W. Lu, Y. Lai, J. Li, L. Zhou, Y. Liu, J. Mater. Chem. 22 (2012) 5560.
[13] J.H. Pikul, P.V. Braun, W.P. King, J. Phys. Conf. Ser. 476 (2013) 012087.
[14] S.J. Dillon, K. Sun, Curr. Opin. Solid State Mater. 16 (2012) 153–162.
[15] X. Zhu, L.-B. Cheng, C.-G. Wang, Z.-P. Guo, P. Zhang, G.-D. Du, H.-K. Liu, J. Phys. Chem. C 113 (2009) 14518–14522.
[16] H. Mazor, D. Golodnitsky, L. Burstein, A. Gladkich, E. Peled, J. Power Sources 198 (2012) 264–272.
[17] V. Palomares, I. Ruiz de Larramendi, J. Alonso, M. Bengoechea, A. Goni, O. Miguel, T. Rojo, Appl. Surf. Sci. 256 (2010) 2563–2568.

Fig. 5. Galvanostatic charge discharge tests at different current rates (0.5, 1, 1.5, 2.5, 5 C) of a) Fe and b) FeMn samples. The Coulombic efficiency is also shown.; c) influence of the current density in μA cm^{-2} (corresponding to 0.5, 1, 1.5, 2.5, 5 C) on the first charge capacity from the 125th cycle onward, (red dots, Fe sample); d) chronopotentiograms of the FeMn sample (13th and 14th cycle of charge–discharge at 0.5 C). (For interpretation of the references to color in this figure legend, the reader is referred to the web version of this article.)

[18] A. Nyten, A. Abouimrane, M. Armand, T. Gustafsson, J.O. Thomas, Electrochem. Commun. 7 (2005) 156–160.
[19] M.S. Islam, R. Dominko, C. Masquelier, C. Sirisopanaporn, A.R. Armstrong, P.G. Bruce, J. Mater. Chem. 21 (2011) 9811–9818.
[20] M. Bini, S. Ferrari, D. Capsoni, C. Spreafico, C. Tealdi, P. Mustarelli, J. Solid State Chem. 200 (2013) 70–75.
[21] M. Bini, S. Ferrari, C. Ferrara, M.C. Mozzati, D. Capsoni, A.J. Pell, G. Pintacuda, P. Canton, P. Mustarelli, Sci. Rep. 3 (2013) 3452, http://dx.doi.org/10.1038/srep03452.
[22] R. Dominko, C. Sirisopanaporn, C. Masquelier, D. Hanzel, I. Arcon, M. Gaberscek, J. Electrochem. Soc. 157 (2010) A1309–A1316.
[23] M.M. Kalantarian, S. Asgari, P. Mustarelli, J. Mater. Chem. A 1 (2013) 2847–2855.
[24] A.R. Armstrong, N. Kuganathan, M.S. Islam, P.G. Bruce, J. Am. Chem. Soc. 133 (2011) 13031–13035.
[25] C. Sirisopanaporn, C. Masquelier, P.G. Bruce, A.R. Armstrong, R. Dominko, J. Am. Chem. Soc. 133 (2011) 1263–1265.
[26] T. Kawase, H. Yoshitake, Microporous Mesoporous Mater. 155 (2012) 99–105.
[27] D. Rangappa, K.D. Murukanahally, T. Tomai, A. Unemoto, I. Honma, Nano Lett. 12 (2012) 1146–1151.
[28] Z. Chen, S. Qiu, Y. Cao, J. Qian, X. Ai, K. Xi, X. Hong, H. Yang, J. Mater. Chem. A 1 (2013) 4988–4992.
[29] R. Dominko, M. Bele, A. Kokalj, M. Gaberscek, J. Jamnik, J. Power Sources 174 (2007) 457.
[30] I. Quinzeni, S. Ferrari, E. Quartarone, P. Mustarelli, J. Power Sources 196 (2011) 10228–10233.
[31] C. Tealdi, E. Quartarone, P. Galinetto, M.S. Grandi, P. Mustarelli, J. Solid State Chem. 199 (2013) 1–6.
[32] X.J. Wu, Z.Z. Zhang, Q.S. Liang, J. Meng, J. Cryst. Growth 340 (2012) 74–77.
[33] Y. Xu, Y. Li, S. Liu, H. Li, Y. Liu, J. Power Sources 220 (2012) 103–107.
[34] J.H. Ku, J.H. Ryu, S.H. Kim, O.H. Han, S.M. Oh, Adv. Funct. Mater. 22 (2012) 3658–3664.
[35] T. Matsuyama, A. Sakuda, A. Hayashi, Y. Togawa, S. Mori, M. Tatsumisago, J. Solid State Electrochem. 17 (2013) 2697–2701.
[36] X. Yu, J.B. Bates, G.E. Jellison, F.X. Hart, J. Electrochem. Soc. 144 (1997) 524–532.
[37] L. Baggetto, N.A.M. Verhaegh, R.A.H. Niessen, F. Roozeboom, J.-C. Jumas, P.H.L. Notten, J. Electrochem. Soc. 157 (2010) A340–A347.
[38] N.J. Dudney, J.B. Bates, R.A. Zuhr, S. Young, J.D. Robertson, H.P. Jun, S.A. Hackney, J. Electrochem. Soc. 146 (1999) 2455–2464.